Renewable Energy, Environment, and Power Quality Journal (REE&PQJ)
ISSN:3020-531X
Volume 26, July 2026

High-Fidelity Co-Simulation and Wind-Grid Coupling Mechanism Analysis of 15 MW Wind Turbines

Bowen Chen, Yonggang Lin, Danyang Li, Zhongpeng Cao, Yajing Gu

The State Key Laboratory of Fluid Power and Mechatronic Systems,
Zhejiang University, Hangzhou 310027, China.
bwer@zju.edu.cn

Abstract. To address the multi-scale dynamic coupling challenges in 15 MW wind turbines, this paper establishes a full-dimensional aerodynamic-mechanical-electrical co-simulation platform integrating OpenFAST, Simpack, and Simulink. A dynamic data-exchange interface and a multi-rate cross-domain co-simulation strategy are proposed to overcome severe numerical stiffness. Based on this platform, the transient electromagnetic torque variations induced by Low Voltage Ride-Through (LVRT) and their impact on drivetrain fatigue are investigated, with a specific focus on the dynamic meshing forces within the gearbox. Preliminary results reveal a strictly phase-dependent nonlinear coupling mechanism: when the grid dip coincides with the falling edge of a wind gust, high-frequency electrical transients constructively interfere with mechanical torsional vibrations, amplifying extreme gearbox loads; conversely, when coinciding with the rising edge of a gust, a destructive interference occurs, where the sustained aerodynamic torque acts as a physical buffer that effectively mitigates the transient mechanical shocks. This study provides a necessary theoretical baseline for subsequent gearbox reliability design and anti-fatigue control under complex multi-source excitations.

Key words. 15 MW Wind Turbine, Multi-body dynamics, Co-simulation, Electromechanical coupling dynamics

1. Introduction

As the unit capacity of wind turbines advances towards the 15 MW level, the compact integrated drivetrain has gradually become the core structural configuration for ultra-large turbines due to its high power density and lightweight advantages. Topologically, this novel architecture achieves a deep integration of the gear system and the generator, completely eliminating the elastic buffering supports (e.g., flexible couplings) found in traditional configurations in favor of a rigid direct-connection mechanism between the output shaft and the generator rotor [1]. Although this highly integrated design significantly reduces the shaft space, it almost entirely removes the physical isolation between the mechanical and electrical sides. Combined with ultra-long flexible blades, the entire turbine exhibits extremely high structural flexibility and low inertia characteristics. In actual service environments, this integrated drivetrain, lacking mechanical damping buffers, is highly sensitive to external disturbances. It not only endures random, broadband aerodynamic loads caused by turbulence and gusts but is also subjected to unattenuated reverse electromagnetic torques from the generator, exhibiting extremely strong multi-source electromechanical coupling dynamics [2],[3].

Under continuous wind disturbances, broadband forced torsional vibrations—highly overlapping with the wind speed fluctuation spectrum—are generated on the drivetrain. Under specific external excitation energies, the electromechanical coupling system of the drivetrain even faces the risk of instability and chaotic oscillation [4]. Under complex grid-connected conditions, grid-side transient faults often evolve into highly destructive high-frequency mechanical shocks. When a voltage dip fault (e.g., LVRT) occurs and enters the recovery phase, the rapid restoration of active power inevitably causes drastic fluctuations in electromagnetic torque, thereby inducing torsional vibrations in the drivetrain and exacerbating the fatigue loads on transmission components [5]. Quantitative studies on such electrical transient-induced mechanical damage indicate that the risk of smearing damage in high-speed bearings increases dramatically by approximately 4.9 times, particularly during converter faults [6],[7].

For the currently dominant Grid-Following (GFL) wind turbines, the transient control and hardware protection actions during LVRT are core triggers for electromechanical coupled torsional vibrations. To meet grid codes and protect converter hardware, additional protection circuits, such as DC chopper circuits or rotor-side crowbars, are typically introduced to dissipate rotor energy and protect the DC bus capacitor [8]. However, the complex control switching during LVRT generates transient surge currents in the rotor. The rapid unloading of electromagnetic torque and nonlinear regulations executed by the converter (e.g., high-frequency switching actions of the Chopper) easily trigger high-frequency electromagnetic torque oscillations and severe deteriorations in speed fluctuations [9]. In practical operations, when an extreme gust coincides with a grid fault that triggers converter protection actions, the aerodynamic and electromagnetic energies collide head-on at the main shaft. Traditional physical analytical models based on quasi-steady and linear superposition assumptions inherently assume a constant load aggravation. However, these models fail to perceive how the specific temporal mismatch (or phase difference) between the aerodynamic wind profile and the electrical transient profoundly dictates whether the electromechanical coupling results in severe nonlinear load amplification or substantial structural load alleviation.

To depict these complex closed-loop dynamic characteristics more comprehensively and evaluate the microscopic fatigue of gearbox components, aero-electro-mechanical multi-physics co-simulation technologies have developed rapidly in recent years. Early explorations include achieving aeroelastic and multibody dynamic co-simulation via FAST and ADAMS to obtain blade root dynamic responses, and integrating FAST with MATLAB/Simscape to evaluate drivetrain loads under electromagnetic transient excitations [10],[11]. Furthermore, Wang et al. developed a tripartite co-simulation environment integrating FAST, ADAMS, and Simulink [12],[13]. However, in the pursuit of higher modeling fidelity, multi-physics co-simulation begins to face severe challenges of cross-scale computational efficiency and numerical stiffness. Therefore, there is a critical need to develop a full-dimensional, high-fidelity co-simulation architecture capable of spanning multiple frequency and time scales to accurately reproduce the transient load evolution process under complex wind-grid coupling conditions.

2. Full-Dimensional Co-Simulation Architecture

The dynamic response of large-scale wind turbines under grid faults is a typical multi-physics coupling problem encompassing aerodynamics, multibody kinematics, and electrical control engineering.To address this cross-scale challenge, a full-dimensional aerodynamic-mechanical-electrical co-simulation platform is established. As comprehensively illustrated in Fig. 1, the overall architecture is constructed by coupling three dominant solvers (OpenFAST, Simpack, and Simulink) through a dynamic data-exchange interface. The specific modeling and coupling formulations are detailed as follows.

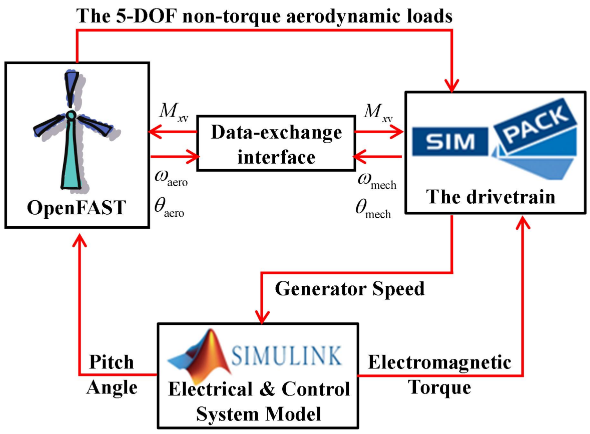

Fig.1. Architecture of the aerodynamic-mechanical-electrical co-simulation platform

A. Subsystem Modeling Strategy

Due to the massive size and structural complexity of the 15 MW turbine, a single simulation software struggles to balance physical comprehensiveness and high fidelity. The proposed platform utilizes dominant solvers in their respective domains for each subsystem:

Aeroelastic Domain (OpenFAST): Responsible for high-fidelity reproduction of the external wind field environment and rotor aeroelastic evolution. It compensates for the oversimplified built-in aerodynamic modules of multibody dynamics software, which struggle to accurately simulate dynamic stall and large-deflection bending of 100-meter ultra-long flexible blades.

Multibody Mechanical Domain (Simpack): Focuses on resolving the internal microscopic multibody topology of the drivetrain. Large components are modeled as flexible bodies using the Craig-Bampton mode synthesis method, and gears are modeled using discrete slicing methods to calculate time-varying mesh stiffness. This resolves the blind spot of traditional aeroelastic software, which simplifies the drivetrain into a two-mass model, failing to observe high-frequency transient internal loads.

Electrical Servo Domain (Simulink): Simulink is introduced as the global master control platform, accurately simulating the actual control logic of the turbine controller. Based on real-time speed and power feedback, Simulink dynamically issues pitch and torque commands, restoring the authentic servo intervention process.

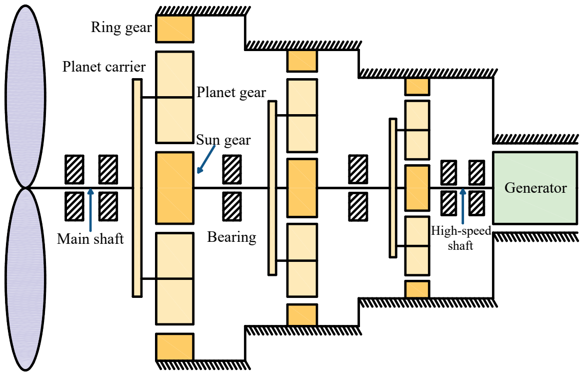

Fig.2. Modeling of the 15 MW integrated wind turbine drivetrain

B. Dynamic Data-Exchange Strategy

To accurately capture the true load transmission path during the wind-grid coupling process, the proposed co-simulation platform establishes bidirectional strong coupling by defining a dynamic data-exchange interface. Within extremely short simulation steps, OpenFAST transmits aerodynamic forces to the downstream Simpack; upon resolving the high-frequency mechanical torsion, Simpack immediately feeds the spatial displacement and velocity of the hub back to the rotor in OpenFAST.

C. Multi-Rate Cross-Domain Co-Simulation Strategy

The wind turbine is a typical cross-time-scale strongly coupled system. Aerodynamic evolution exhibits extreme low-frequency characteristics (<3 Hz), drivetrain multibody dynamics dominate low-to-medium frequency torsion and vibration (1~100 Hz), and grid electromagnetic transients exhibit high-frequency characteristics (⩾ 50 Hz). Forcing a single solver to process them simultaneously easily triggers numerical stiffness and divergence.

This study adopts a Multi-rate Co-simulation strategy in the architecture:

Electrical Micro-Step: Considering the 50 Hz fundamental transient and electromagnetic coupling effects, the Simulink solver step size is set to 0.0001 s, utilizing an Average-Value Model (AVM) to effectively filter switching noise.

Global Communication Step: The global communication step between OpenFAST and Simpack is set to 0.001 s (1000 Hz), effectively avoiding high-frequency aliasing.

Internal Variable Step: Simpack internally utilizes a variable-step implicit integrator (SODASRT 2) to adaptively handle high-frequency nonlinear gear contacts with minimal steps.

This fundamental physical decoupling and computational allocation mechanism resolves the numerical stiffness contradiction of strongly coupled systems from the bottom up, ensuring global stability under extreme transient conditions.

3. Preliminary Results and Mechanism Analysis

Based on the established high-fidelity platform, the time-domain characteristics of the interaction between aerodynamic loads and electrical transient loads under a typical LVRT scenario are analyzed. To accurately evaluate the microscopic fatigue damage inside the gearbox, this study extracts the peak-to-peak amplitude envelope of the dynamic normal meshing force, denoted as F_{p2p}, between the sun and planet gears in the intermediate stage using a 0.5-second sliding time window. This specific location is selected because the intermediate planetary stage acts as the critical load-transfer bottleneck within the highly integrated drivetrain; it directly confronts the violent superposition of massive low-frequency aerodynamic torque and unattenuated high-frequency electromagnetic transient shocks, making it highly vulnerable to fatigue failure under complex electromechanical coupling.

$$F_{\text{p2p}}(t) = F_{\text{N}}^{\max}(t) - F_{\text{N}}^{\min}(t) \tag{1}$$

where $F_{\text{N}}^{\max}(t)$ and $F_{\text{N}}^{\min}(t)$ represent the local upper and lower envelope values of the meshing force.

To isolate the nonlinear coupling effects, a baseline linear prediction is constructed by superimposing the transient increments derived from independent single-excitation scenarios. Specifically, a nominal response is first established under completely normal operating conditions. The transient load increments induced by the pure extreme gust and the pure grid fault are separately calculated relative to this nominal baseline. The linear prediction, $F_{\text{p2p}}^{\text{lin}}$, is then formulated by superimposing these two independent dynamic increments onto the normal baseline. This provides a mathematically rigorous reference under the assumption that aerodynamic and electromagnetic excitations do not interact.

Furthermore, a dual-verification diagnostic framework is established based on the Ultimate Limit State (ULS) and Fatigue Limit State (FLS). The ULS represents the maximum transient shock extracted from the envelope, defined mathematically as:

$$L_{\text{ULS}} = \max(F_{\text{p2p}}) \tag{2}$$

In contrast, the FLS denotes the cumulative damage obtained via time integration of the envelope over the statistical period T_{stat}:

$$E_{\text{FLS}} = \int_{T_{\text{stat}}} F_{\text{p2p}}(t)dt \tag{3}$$

Two specific indices are subsequently defined to evaluate the electromechanical coupling effect. First, the Engineering Hazard Ratio H evaluates the load aggravation multiple of the actual coupled response compared to the pure LVRT response:

$$H_{\text{ULS}} = \frac{L_{\text{ULS}}^{\text{cpl}}}{L_{\text{ULS}}^{\text{lvrt}}}, \quad H_{\text{FLS}} = \frac{E_{\text{FLS}}^{\text{cpl}}}{E_{\text{FLS}}^{\text{lvrt}}} \tag{4}$$

Second, the Physical Nonlinearity Coefficient Γ compares the actual coupled response against the linear superposition prediction:

$$\Gamma_{\text{ULS}} = \frac{L_{\text{ULS}}^{\text{cpl}}}{L_{\text{ULS}}^{\text{lin}}}, \quad \Gamma_{\text{FLS}} = \frac{E_{\text{FLS}}^{\text{cpl}}}{E_{\text{FLS}}^{\text{lin}}} \tag{5}$$

A coefficient Γ greater than 1.0 mathematically falsifies the linear superposition assumption, indicating constructive interference and nonlinear amplification. Conversely, a value below 1.0 signifies destructive interference and load suppression. Applying this diagnostic framework, the preliminary results reveal a strictly phase-dependent electromechanical coupling mechanism.

A. Grid Dip Occurs During Gust Falling Edge

As depicted in Fig. 3(a), the LVRT triggers during the descent phase of the extreme gust. To explicitly illustrate this transient process, Fig. 3(b) presents the dynamic responses, where the blue shaded background denotes the extreme gust duration and the vertical red dashed lines indicate the LVRT window. The upper panel compares the F_{p2p} envelopes under pure LVRT, linear prediction, and actual coupled conditions. It is visually evident that the actual coupled response significantly exceeds the linear prediction. Physically, the Grid-Following controller rapidly reduces active current, causing a sudden loss of electromagnetic counter-torque, which forces the drivetrain to experience a violent torsional rebound. To further quantify this deviation, the bottom panel isolates the nonlinear difference. As highlighted by the red shaded areas in the difference curve, the high-frequency electrical ripples directly superimpose onto the low-frequency mechanical torsional oscillation peaks. Evaluated by the proposed framework and quantitatively summarized in Fig. 3(c), the gearbox meshing force exhibits an ULS Hazard Ratio of 1.169X (a nearly 17% amplification) and an FLS Energy Ratio of 1.165X. The physical nonlinearity indices—specifically $\Gamma_{\text{ULS}} = 1.054$ and $\Gamma_{\text{FLS}} = 1.078$ —are strictly greater than 1.0. This statistically proves a pronounced nonlinear amplification effect, severely aggravating the transient fatigue loads on the gear teeth.

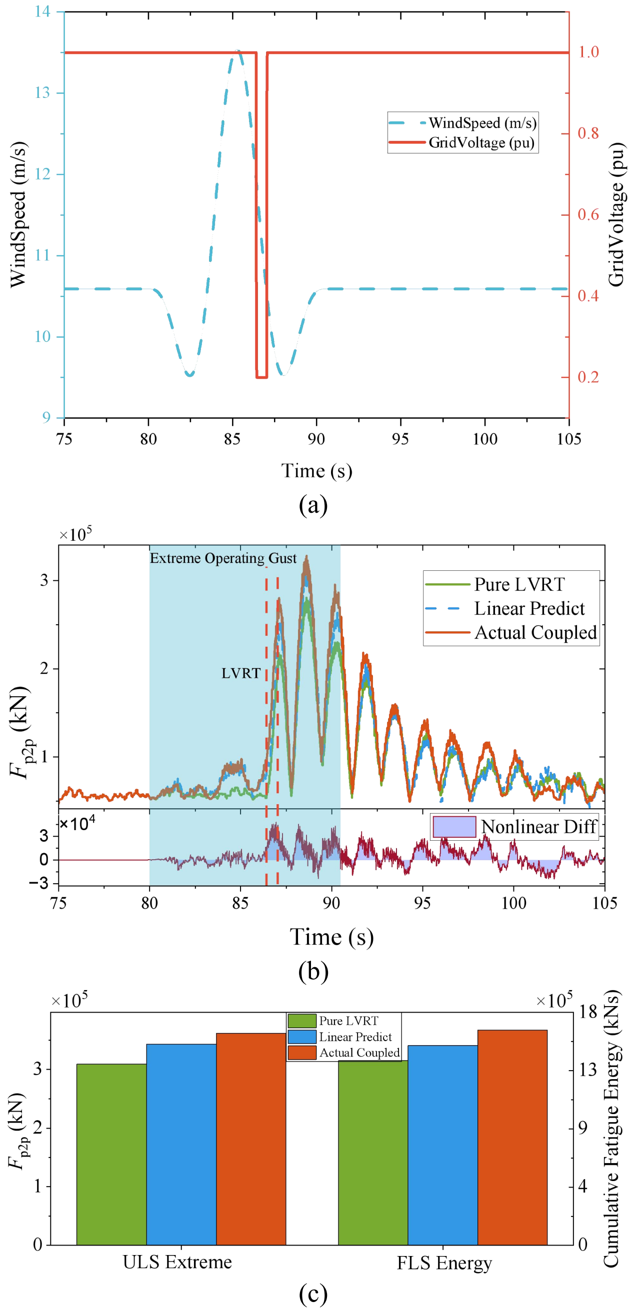

Fig.3. Electromechanical coupling dynamics when the grid dip occurs during the gust falling edge: (a) Macroscopic boundary conditions; (b) Transient meshing force envelope (F_{p2p}) and nonlinear difference highlighting constructive interference; (c) Damage quantification of ULS extreme and FLS energy.

B. Grid Dip Occurs During Gust Rising Edge (Destructive Interference)

Conversely, when the LVRT coincides with the rising edge of the gust, a distinctly opposing physical phenomenon is observed. As shown in the upper panel of Fig. 4(b), the actual coupled F_{p2p} response is markedly lower than the linear prediction. Although the electromagnetic torque drops abruptly, the synchronously increasing aerodynamic thrust and torque act as a powerful aerodynamic damper. This continuous forward tension restrains the flexible main shaft from violent structural snap-back. As extracted in the bottom panel of Fig. 4(b), the blue shaded areas in the nonlinear difference curve verify this load attenuation, demonstrating that the strong aerodynamic load dynamically neutralizes the electrical transients. Data manifests that both engineering hazard and physical nonlinearity inside the gearbox are significantly suppressed. As shown in the comparative bars of Fig. 4(c), the ULS Hazard Ratio drops to 0.805X, and Γ_{ULS} decreases to 0.765. With all diagnostic ratios falling below 1.0, a destructive interference mechanism is verified, leading to a substantial attenuation of the gearbox fatigue energy with $\Gamma_{FLS} = 0.856$.

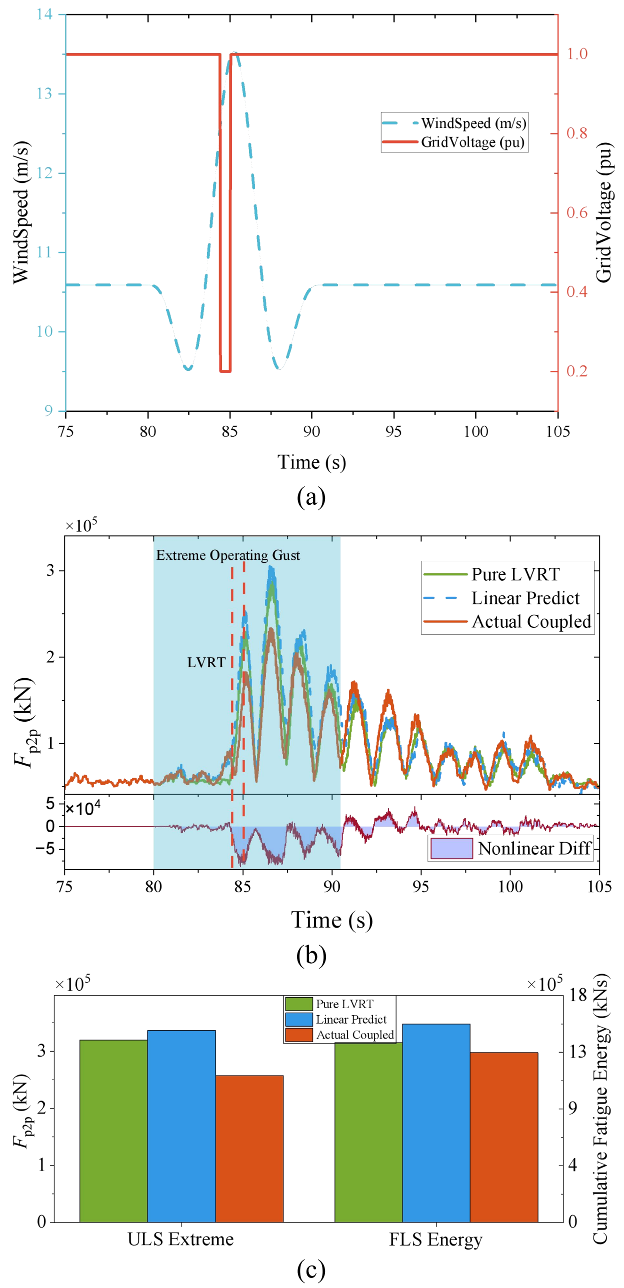

Fig. 4. Electromechanical coupling dynamics when the grid dip occurs during the gust rising edge: (a) Macroscopic boundary conditions; (b) Transient meshing force envelope (F_{p2p}) and nonlinear difference highlighting destructive interference; (c) Damage quantification of ULS extreme and FLS energy.

4. Conclusion

This paper establishes a high-fidelity, cross-scale multi-rate co-simulation environment for 15 MW integrated wind turbines. The proposed dynamic data-exchange interface and the "micro-step, macro-step, variable-step" synergistic solving strategy effectively resolve the time-scale barriers and numerical stiffness bottlenecks between heterogeneous solvers. Preliminary time-domain simulations and quantitative diagnostics unveil a crucial phase-dependent coupling mechanism: the temporal mismatch between grid fault-induced electromagnetic torque dips and delayed aerodynamic pitch actions fundamentally dictates the severity of gearbox damage. When occurring during a gust falling edge, high-frequency electrical ripples constructively interfere with mechanical torsional rebounds, nonlinearly amplifying extreme gear meshing loads by nearly 17%; however, during a gust rising edge, the sustained aerodynamic torque provides destructive interference, which effectively suppresses the ultimate loads. The electromechanical coupled transient characteristics revealed in this paper provide a solid theoretical foundation for the future structural optimization and advanced transient control strategy design of large-scale wind turbines.

Acknowledgement

This work was supported by the National Key R&D Program of China (Grant No. 2023YFB4203000) and the National Natural Science Foundation of China (Grant No. U22A20178).

References

[1] Yang, S., Zhu, C., Li, C., Zhou, Y., Tan, J., & Liao, B. (2025). Physics-data hybrid dynamic analysis of novel integrated wind turbine drivetrain. International Journal of Mechanical Sciences, 302, 110564.
[2] Nejad, A. R., Keller, J., Guo, Y., Sheng, S., Polinder, H., Watson, S., ... & Bergman, J. (2022). Wind turbine drivetrains: state-of-the-art technologies and future development trends. Wind Energy Science, 7(1), 387-398.
[3] Chen, R., Qin, D., Yi, Y., Liu, C., & Shi, J. (2022). Dynamic characteristics of electromechanical coupling of wind turbine drive system under multi-source excitation. Wind Energy, 25(3), 391-418.
[4] Yang, J., Zhou, F., Xiong, J., Hou, Z., Zhang, J., & Mu, A. (2023). Torsional vibration characteristics analysis and adaptive fixed-time control of wind turbine drivetrain. Energy Science & Engineering, 11(12), 4666-4686.
[5] Guang, C., Xiangwu, Y., Shurui, Z., Haoyang, R., Jiaoxin, J., & Fan, Z. (2026). Dynamic active torque coordination strategy for torsional vibration suppression in wind turbines during grid fault recovery. International Journal of Electrical Power & Energy Systems, 175, 111590.
[6] Roeder, J., Jacobs, G., Duda, T., Bosse, D., & Herzog, F. (2021). Investigation of dynamic loads in wind turbine drive trains due to grid and power converter faults. Energies, 14(24), 8542.
[7] Fateh, F., White, W. N., & Gruenbacher, D. (2017). Torsional vibrations mitigation in the drivetrain of DFIG-based grid-connected wind turbine. IEEE Transactions on Industry Applications, 53(6), 5760-5767.
[8] Haidar, A. M. A., Muttaqi, K. M., & Hagh, M. T. (2017). A coordinated control approach for DC link and rotor crowbars to improve fault ride-through of DFIG-based wind turbine. IEEE Transactions on Industry Applications, 53(4), 4073-4086.
[9] Rahimi, M., & Parniani, M. (2010). Grid-fault ride-through analysis and control of wind turbines with doubly fed induction generators. Electric Power Systems Research, 80(2), 184-195.
[10] Girsang, I. P., Dhupia, J. S., Muljadi, E., Singh, M., & Pao, L. Y. (2014). Gearbox and Drivetrain Models to Study Dynamic Effects of Modern Wind Turbines. IEEE Transactions on Industry Applications, 50(6), 3777-3786.
[11] Du, J., Hou, H. C., & Wang, Z. (2013). Simulation Analysis of Gear Box of Wind Turbine Based on Flexible Multi-body Dynamics. Metalurgia International, 18(3), 116-121.
[12] Wang, C. S., & Chiang, M. H. (2016). A Novel Dynamic Co-Simulation Analysis for Overall Closed Loop Operation Control of a Large Wind Turbine. Energies, 9(8).
[13] Chiang, M. H., Wang, C. S., Tung, T. C., et al. (2015). Development of Co-simulation and Analysis by Combination of Aerodynamics, Mechanism Dynamics and Control System Dynamics for Large Wind Turbines. Proceedings of the AASRI International Conference on Industrial Electronics and Applications, 2, 348-351.